

Assessment of Arctic Sea Ice and Surface Climate Conditions in Nine CMIP6 Climate Models

Martin Henke¹, Celso M Ferreira¹, Jinlun Zhang², Thomas Ravens³, Tyler Will Miesse¹, and Felício Cassalho¹

¹George Mason University

²Polar Science Center, Applied Physics Lab, University of Washington

³University of Alaska Anchorage

December 21, 2022

Abstract

The observed retreat and anticipated further decline in Arctic sea ice hold strong climate, environmental, and societal implications. In predicting climate evolution, ensembles of coupled climate models have demonstrated appreciable accuracy in simulating sea ice area and volume trends throughout the historical period. However, individual climate models still show significant differences in simulating the sea ice thickness distribution. To better understand individual model performance in sea ice simulation, nine climate models previously identified to provide plausible sea ice decline and global temperature change were evaluated in comparison with Arctic satellite and reanalysis derived sea ice thickness data, sea ice extent records, and atmospheric reanalysis data of surface wind and air temperature. Assessment found that the simulated spatial distribution of historical sea ice thickness varies greatly between models and that several key limitations persist among models. Primarily, most models do not capture the thickest regimes of multi-year ice present in the Wandel and Lincoln Seas; those that do, often possess erroneous positive bias in other regions such as the Laptev Sea or along the Eurasian Arctic Shelf. From analysis, no model could be identified as performing best overall in simulating historic sea ice, as model bias varies regionally and seasonally. Nonetheless, the bias maps and statistical measures derived from this analysis should enhance understanding of the limitations of each climate model. This research is motivated in-part to inform future usage of coupled climate model projection for regional modeling efforts and enhance climate change preparedness and resilience in the Arctic.

Hosted file

951574_0_art_file_10547851_rn55sq.docx available at <https://aurea.com/users/568346/articles/614224-assessment-of-arctic-sea-ice-and-surface-climate-conditions-in-nine-cmip6-climate-models>

18 **Abstract**

19 The observed retreat and anticipated further decline in Arctic sea ice holds strong climate,
20 environmental, and societal implications. In predicting climate evolution, ensembles of coupled
21 climate models have demonstrated appreciable accuracy in simulating sea ice area and volume
22 trends throughout the historical period. However, individual climate models still show significant
23 differences in simulating the sea ice thickness distribution. To better understand individual
24 model performance in sea ice simulation, nine climate models previously identified to provide
25 plausible sea ice decline and global temperature change were evaluated in comparison with
26 Arctic satellite and reanalysis derived sea ice thickness data, sea ice extent records, and
27 atmospheric reanalysis data of surface wind and air temperature. Assessment found that the
28 simulated spatial distribution of historical sea ice thickness varies greatly between models and
29 that several key limitations persist among models. Primarily, most models do not capture the
30 thickest regimes of multi-year ice present in the Wandel and Lincoln Seas; those that do, often
31 possess erroneous positive bias in other regions such as the Laptev Sea or along the Eurasian
32 Arctic Shelf. From analysis, no model could be identified as performing best overall in
33 simulating historic sea ice, as model bias varies regionally and seasonally. Nonetheless, the bias
34 maps and statistical measures derived from this analysis should enhance understanding of the
35 limitations of each climate model. This research is motivated in-part to inform future usage of
36 coupled climate model projection for regional modeling efforts and enhance climate change
37 preparedness and resilience in the Arctic.

38 **Plain Language Summary**

39 The expected future decline in Arctic sea ice will have far-reaching global impacts. In simulating
40 sea ice, many global climate models have shown skill in predicting the seasonal cycle and area of
41 sea ice, yet struggle in simulating sea ice thickness. This study evaluates the ability of nine
42 climate models to simulate sea ice thickness in different Arctic regions and months. This is
43 accomplished by comparing historical climate model simulations to reference data such as
44 satellite observations. Additionally, model simulations of sea ice extent and climate variables
45 related to sea ice dynamics (surface wind speed and air temperature) are assessed to provide
46 insight into related and driving variables. From this process, we found that while sea ice
47 thickness varies substantially between models, there are some common areas that models
48 struggle to simulate. Namely, sea ice thickness is often too thin in the Wandel and Lincoln Seas,
49 and too thick in the Laptev Sea or along the Eurasian Arctic Shelf. No single model is identified
50 as best due to changing performance depending on season and region. However, this analysis
51 should give insight of model performance for those interested in utilizing climate model
52 simulations for predicting climate change in the Arctic.

53

54 **1 Introduction**

55 Arctic sea ice has declined dramatically over the previous century, foremost
56 demonstrated by a persistent negative trend in sea ice area from 1979 to the present (Doscher et
57 al., 2014; Laxon et al., 2013; Julienne Stroeve & Notz, 2018). Thinning of sea ice regimes has
58 also been confirmed, as the prevalence of perennial multi-year ice has diminished, being
59 replaced by seasonal first-year ice (Kwok, 2018; Maslanik et al., 2007; Julienne Stroeve & Notz,
60 2018). This first-year sea ice is: i) thinner than perennial sea ice (Tschudi et al., 2016), ii) more

61 dynamic (Kwok et al., 2013; Olason & Notz, 2014), and iii) further responsive to atmospheric
62 and oceanic forcing (Kwok, 2018; Overland, 2020). Sea ice plays a critical role in Arctic
63 atmosphere and ocean processes; modifying the thermal energy budget through high surface
64 albedo and suppressing air-sea heat, moisture, and momentum fluxes (Mercè Casas-Prat &
65 Wang, 2020; Goosse et al., 2018; Haine et al., 2015; Karlsson & Svensson, 2013; Mioduszewski
66 et al., 2018; Julienne Stroeve & Notz, 2018; Thomson & Rogers, 2014; Timmermans &
67 Marshall, 2020). Beyond geophysical effects, reduced Arctic sea ice cover is anticipated to have
68 considerable societal effects with potential increases in Arctic maritime activity (Aksenov et al.,
69 2017; Chen et al., 2020; Sibul & Jin, 2021), growing regional development (Harsem et al., 2015),
70 and greater risk of coastal hazards to impact Arctic communities (Barnhart et al., 2014;
71 Mioduszewski et al., 2018; Williams & Erikson, 2021). As the reality of an “ice-free” summer
72 (sea ice area less than 1×10^6 km²) is predicted to occur before 2050 (Chen et al., 2020; SIMIP
73 Community, 2020; Wei et al., 2020), accurate forecasting of sea ice is crucial to facilitate
74 understanding and preparedness for future impacts.

75 Climate models participating in the Coupled Model Intercomparison Project’s sixth phase
76 (CMIP6) have shown marked improvement in simulating sea ice cover in comparison to prior
77 phases. The multimodel mean of sea ice extent (SIE) generally captures the seasonal amplitude
78 between March peak SIE and the September low. Yet, most models underestimate the observed
79 downward trend of sea ice extent, and there is a wide intermodel spread during the summer
80 months when the greatest negative trend occurs (Long et al., 2021; Shen et al., 2021; Shu et al.,
81 2020; SIMIP Community, 2020). Even models shown to best follow the observed seasonal sea
82 ice area and volume still experience numerous challenges in simulating the spatial distribution of
83 sea ice thickness (Davy & Outten, 2020; Watts et al., 2021).

84 This research seeks to assess CMIP6 climate models’ skill in simulating historic sea ice
85 thickness, extent, and related surface climate variables in order to identify potential candidates
86 for future dynamic downscaling. Intensive effort has been directed towards analyzing CMIP6
87 models’ sea ice cover simulation in the interest of improving climate projection (Shen et al.,
88 2021; Shu et al., 2020; SIMIP Community, 2020; Watts et al., 2021). Accurate forecasts of sea
89 ice are crucial to Arctic stakeholders impacted by changing sea ice conditions and dependent
90 Arctic research efforts such as wave projections (M. Casas-Prat et al., 2018) or arctic maritime
91 accessibility studies (Chen et al., 2020; Melia et al., 2016). By enhancing understanding of
92 model simulation of sea ice and related surface climate variables (wind speed and surface air
93 temperature), this research is intended to provide a resource for future Arctic research reliant on
94 the accuracy of climate model projections. It should be recognized that accurate simulation of
95 historic conditions does not guarantee future projection accuracy. However, the inverse,
96 consistent bias in simulating historical conditions does imply model shortcomings, and thus the
97 process of model selection using historical performance criteria is necessary and has been shown
98 to significantly influence the trajectory of future projections (Docquier & Koenigk, 2021; Knutti
99 et al., 2017).

100 To assess model simulation, historic Arctic sea ice and related surface climate variables
101 were evaluated from the beginning of the satellite era to the end of the CMIP6 historical
102 experiment (1979-2014). The sea ice variables assessed included sea ice thickness (SIT) and sea
103 ice extent (SIE), and the surface climate variables assessed included surface wind speed (SWS)
104 and surface air temperature (SAT). SWS and SAT were selected for analysis because they are
105 important sea ice drivers and have Pan-Arctic availability and reasonable accuracy from

106 atmospheric reanalysis products. These variables were compared monthly with remote sensing
 107 derived data, reanalysis sea ice products, and atmospheric reanalysis products. SIT simulation
 108 was evaluated in comparison to both the Pan-Arctic Ice Ocean Modeling and Assimilation
 109 System (PIOMAS) sea ice thickness reanalysis and merged CryoSat-2-SMOS sea ice thickness
 110 measurements 2011- 2014. The National Snow and Ice Data Center (NSIDC) Sea Ice Index (SII)
 111 was used to assess model simulation of average monthly SIE and trends. Finally, ERA5
 112 atmospheric reanalysis was used in assessing model simulation of both SAT and SWS variables.
 113 Supplementing the Pan-Arctic analysis, model simulation of SIT within the Canadian
 114 Archipelago and the nearby Baffin Bay was analyzed.

115 2 Data and Methods

116 2.1 Model Selection

117 Models selected for evaluation were identified from a previous assessment that identified
 118 models which forecast a realistic amount of sea ice loss while concurrently simulating a plausible
 119 global mean temperature change (SIMIP Community, 2020). The nominal horizontal resolution
 120 of the analyzed climate models differs substantially. Model resolution has been found to
 121 influence the accuracy of models, with higher resolution models tending to exhibit better
 122 simulation of oceanic heat transfer (Docquier et al., 2019). The CMIP6 historical experiment
 123 provides historical simulation data in varying temporal resolution; in this research, monthly
 124 averages of simulated variables were assessed. Multiple simulation realizations are available for
 125 all but two of the models evaluated as shown in Table 1. These two models: CNRM-CM6-1-HR
 126 and GFDL-ESM4, have only one available realization member, and thus robust conclusions
 127 pertaining to either model's physics are indeterminate. However, this does not negate the
 128 performance of the individual realization.

130 **Table 1. Climate models evaluated within the study, individual ocean grid resolution,**
 131 **affiliated institution, and the number of ensemble members available/used.**

Climate Model	Sea Ice Grid Resolution	Institution ID	Ensemble Members
ACCESS-CM2	360 × 300	CSIRO-ARCCSS	5
CESM2-WACCM	384 × 324	NCAR	3
CNRM-CM6-1-HR	1442 × 1050	CNRM-CERFACS	1
GFDL-ESM4	720 × 576	NOAA-GFDL	1
GISS-E2-2-G	90 × 144	NASA-GISS	10
MPI-ESM-1-2-HAM	256 × 220	MPI-M	3
MPI-ESM-1-2-HR	404 × 802	HAMMOZ-Consortium	10
MRI-ESM2-0	363 × 360	MRI	10
NorESM2-MM	360 × 384	NCC	3

132 2.2 Sea Ice Evaluation

133 SIT accuracy is assessed through comparison with the Alfred Wegner Institute's
 134 combined CryoSat-SMOS (CS2SMOS) Merged Sea Ice Thickness data product (Ricker et al.,
 135 2017) and PIOMAS sea ice reanalysis dataset. The merged satellite data product utilizes both
 136 CryoSat-2 and SMOS derived SIT measurements. The combined analysis SIT product is

137 enhanced to measure a greater range of sea ice thickness regimes – most notably thin ice from
138 SMOS (Kwok & Cunningham, 2015; X. Wang et al., 2016). The CS2SMOS SIT product
139 provides monthly coverage from October through April. However, full monthly data for October
140 and April is incomplete, with the dataset beginning in late October and terminating in early
141 April; this may potentially introduce a positive and negative bias for both monthly means
142 respectively. The overlap between complete CS2SMOS data and the CMIP6 historical
143 experiment begins in 2011 and ends in 2014. Given the brevity in this period of assessment, and
144 the inclusion of 2012 – the anomaly lowest summer SIE on record - an additional basis of
145 assessment was needed to evaluate the mean distribution of sea ice. For this purpose, the Pan-
146 Arctic Ice Ocean Modeling and Assimilation System (PIOMAS) sea ice thickness reanalysis is
147 used for SIT comparison monthly 1979 – 2014 (A. Schweiger et al., 2011; Zhang & Rothrock,
148 2003). PIOMAS provides monthly full-year coverage and allows for the annual sea ice minimum
149 occurring in September to be analyzed.

150 The process of model SIT comparison is described as follows: i) the average was taken
151 across ensemble members, ii) monthly sea ice grids were linearly interpolated onto either the
152 CS2SMOS or PIOMAS grid, iii) months were averaged across the entire analysis period
153 establishing a month SIT mean, and iv) model and reference grids were subtracted to create error
154 maps and derive statistical measures. Grid cells where both model and reference agree on open
155 water conditions were excluded from the derivation of statistical measures to reduce the effect of
156 large open water areas during summer months. Following Pan-Arctic analysis, regional analysis
157 for the Canadian Archipelago was performed, and summary statistics were derived for the area.
158 Regional analysis limits analysis to the coordinates between latitudes 60°N to 80°N and
159 longitudes 50°W to 130°W which effectively encompasses the Canadian Archipelago and Baffin
160 Bay.

161 Evaluation of climate model SIE is assessed with monthly SIE values reported from the
162 NSIDC's Sea Ice Index (Meier et al., 2017; Peng et al., 2013). Arctic SIE is defined as the total
163 Arctic area possessing a minimum of 15% sea ice concentration (SIC). Each model's native grid
164 was used to derive SIE, then the average of all realizations was taken to create the ensemble
165 mean SIE time series. These values are then compared with the NSIDC Sea Ice Index value to
166 determine bias.

167 2.3 Surface Climate Evaluation

168 The European Center for Medium Range Forecasts' ERA5 atmospheric reanalysis
169 provides reference for SAT and SWS simulation analysis. Both surface air temperature and
170 surface wind speed were analyzed in comparison to ERA5 historical atmospheric climate
171 reanalysis data product. In a study of atmospheric reanalysis products within the Arctic, ERA5 or
172 ERA-interim (predecessor to ERA5) simulated SAT and SWS were found to have high
173 correlation and low error in comparison to the observed Arctic surface climate, thus qualifying
174 the reanalysis for use in comparison (Demchev et al., 2020; Graham et al., 2019; Lindsay et al.,
175 2014). However, it should be noted that ERA5 possesses a warm bias under extremely cold
176 winter conditions (Davy & Outten, 2020; Demchev et al., 2020; Graham et al., 2019; C. Wang et
177 al., 2019).

178 **3 Results**179 **3.1 Sea Ice Thickness**

180 The European Center for Medium Range Forecasts' ERA5 atmospheric reanalysis
181 provides reference for SAT and SWS simulation analysis. Both surface air temperature and
182 surface wind speed were analyzed in comparison to ERA5 historical atmospheric climate
183 reanalysis data product. In a study of atmospheric reanalysis products within the Arctic, ERA5 or
184 ERA-interim (predecessor to ERA5) simulated SAT and SWS were found to have high
185 correlation and low error in comparison to the observed Arctic surface climate, thus qualifying
186 the reanalysis for use in comparison (Demchev et al., 2020; Graham et al., 2019; Lindsay et al.,
187 2014). However, it should be noted that ERA5 possesses a warm bias under extremely cold
188 winter conditions (Davy & Outten, 2020; Demchev et al., 2020; Graham et al., 2019; C. Wang et
189 al., 2019).

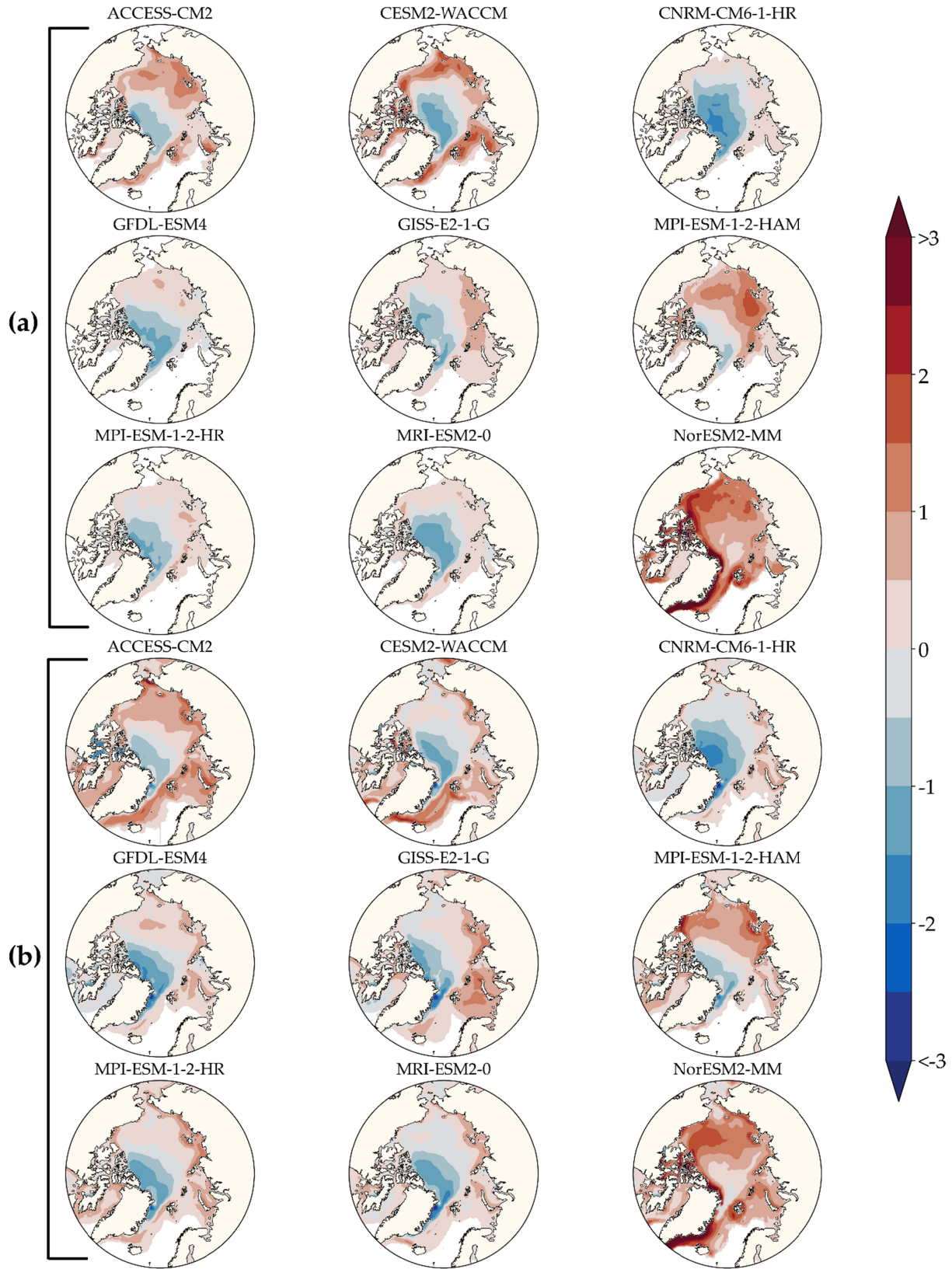
190 Comparison of model-simulated monthly SIT and averaged CS2SMOS observations for
191 October and March over the four-year period 2011-2014 yields bias plots for October (Fig. 1a)
192 and March (Fig. 1b). The summary statistics for both months are presented in Table 2 along with
193 the overall statistics averaged over October through April. CS2SMOS data is unavailable for the
194 annual sea ice minimum month (September) and does not start until the latter half of the month
195 of October. This potentially introduces a positive SIT bias into the month's average used for
196 comparison. Despite this, over half the models exhibit a positive bias for October, ranging from
197 16cm to over 1m. For most models, this stems from an erroneous region of thick sea ice in
198 Eastern Siberian and Chukchi Seas, most pronounced in the ACCESS-CM2, CESM2-WACCM,
199 MPI-ESM-1-2-HAM, and NorESM2-MM models. This phenomenon has been previously
200 observed as common to the majority of CMIP5 models analyzed (J. Stroeve et al., 2014), and it
201 is notable that several models do not possess this feature. The three models with the highest
202 mean positive bias for October are CESM2-WACCM, MPI-ESM-1-2-HAM, and NorESM2-MM
203 having mean bias values of 0.31m, 0.44m, 1.06m respectively. CESM2-WACCM incorrectly
204 calculates a region of very thick ice (>2m) at the outer edge of the sea ice areas for October. It
205 also simulates extremely thick ice (>6m) at several locations within the Canadian Archipelago.
206 MPI-ESM-1-2-HAM shows positive bias (>1m) near the Laptev Sea and NorESM2-MM model
207 has significant positive bias throughout the Arctic.

208 Previous climate model evaluations have shown models typically underestimate
209 especially thick sea ice regimes. This holds true with the majority of models evaluated which
210 undercalculated the thick multi-year ice observed at the Wandel Sea, Lincoln Sea, and north of
211 the Canadian Archipelago. CESM2-WACCM is able to simulate part of the sea ice regime
212 occurring along the northern coast of Greenland; yet it underestimates the continuation of the
213 field towards the pole. MPI-ESM-1-2-HAM shows only slight underestimation ($\approx -0.5\text{m}$) of the
214 thickest sea ice region during October, with bias growing into March. The only model to
215 overrepresent ice in this region is the NorESM2-MM model, which shows significant positive
216 bias throughout the Arctic. Recent research has shown the multi-year ice dominant in this region
217 is more vulnerable to climate change than previously thought (A. J. Schweiger et al., 2021), and
218 thus may be more responsive to climatic forcing (Overland, 2020). In March, nearly all models
219 show improved spatial correlation in comparison to October – as models typically struggle to
220 capture the annual sea ice minimum. Conversely, GISS-E2-1-G spatial correlation drops
221 significantly from 0.72 to 0.51 from October to March; this is primarily attributed to significant

222 overestimation of March sea ice area far into southern Bering Sea and extending into the Pacific
 223 Ocean. All models show positive bias of varying magnitude and extent in the Laptev Sea and
 224 commonly extending into the Eastern Siberian Sea. Models maintaining a correlation of $r \geq 0.8$
 225 overall are CNRM-CM6-1-HR, GFDL-ESM4, MPI-ESM-1-2-HAM, and MPI-ESM-1-2-HR. Of
 226 these, MPI-ESM-1-2-HR shows the lowest mean bias and the highest correlation coefficient.

227 **Table 2. Statistics of error between each model's ensemble average and the reference**
 228 **CS2SMOS Analysis SIT for the individual months of October and March; and an average**
 229 **of winter months (October through April) 2011 to 2014. RMSE and Mean Bias have a unit**
 230 **of meters.**

MODEL	ACCESS- CM2	CESM2- WACCM	CNRM- CM6-1-HR	GFDL- ESM4	GISS- E2-1-G	MPI-ESM- 1-2-HAM	MPI-ESM- 1-2-HR	MRI- ESM2-0	NorESM 2-MM
OCTOBER									
<i>RMSE</i>	0.62	0.93	0.68	0.52	0.35	0.72	0.46	0.53	1.41
<i>MEAN BIAS</i>	0.27	0.31	-0.34	-0.19	0.17	0.44	-0.09	-0.10	1.06
<i>R</i>	0.66	0.28	0.77	0.80	0.72	0.72	0.85	0.74	0.65
MARCH									
<i>RMSE</i>	0.68	0.77	0.57	0.57	0.90	0.66	0.55	0.58	1.16
<i>MEAN BIAS</i>	0.34	0.22	-0.13	-0.09	0.66	0.29	0.08	0.08	0.80
<i>R</i>	0.79	0.67	0.83	0.81	0.51	0.83	0.82	0.79	0.76
AVERAGE (OCT – APR)									
<i>RMSE</i>	0.64	0.76	0.58	0.53	0.72	0.64	0.51	0.54	1.18
<i>MEAN BIAS</i>	0.28	0.15	-0.20	-0.12	0.48	0.30	0.01	-0.03	0.81
<i>R</i>	0.77	0.61	0.80	0.80	0.54	0.81	0.82	0.78	0.74



233 **Figure 1. Sea ice thickness bias (meters) between model ensemble mean and CS2SMOS for**
 234 **October (a) and March (b), over the period 2011-2014.**

235 Supplementing the comparison via CS2SMOS data, climate models were evaluated using
 236 the extended PIOMAS sea ice reanalysis 1979 – 2014. Differing in this step of assessment –
 237 September monthly averages are compared rather than October used for CS2SMOS. Almost all
 238 models show increased agreement with PIOMAS; suspected drivers of this result include the
 239 lengthened time series, and the fact that PIOMAS itself exhibits bias in several regions common
 240 to climate models including the aforementioned positive bias in the Eastern Siberian and
 241 Chukchi seas (J. Stroeve et al., 2014). Three models (ACCESS-CM2, CESM2-WACCM, MPI-
 242 ESM-1-2-HAM) simulate the thick sea ice north of Greenland with negative bias less than >1m
 243 in both March and September; all other models underpredict SIT in this region with exception of
 244 NorESM2-MM possessing a Pan-Arctic positive bias. Similar to the CS2SMOS comparison for
 245 October, CESM2-WACCM again has erroneous high SIT at the outer edge of September Sea ice
 246 area which drives low correlation and high bias. While MPI-ESM-1-2-HR performed best in
 247 comparison to CS2SMOS overall, MPI-ESM-1-2-HAM and GISS-E2-1-G perform markedly
 248 better in comparisons to PIOMAS. The improved correlation of GISS-E2-1-G is notable, as this
 249 model exhibited the lowest correlation with CS2SMOS data. Further inspection into this result
 250 shows that this model exhibits negative bias in comparison to PIOMAS and large positive bias in
 251 comparison to the CS2SMOS data; suggesting that the model may not capture the thinning of sea
 252 ice regimes in later years.

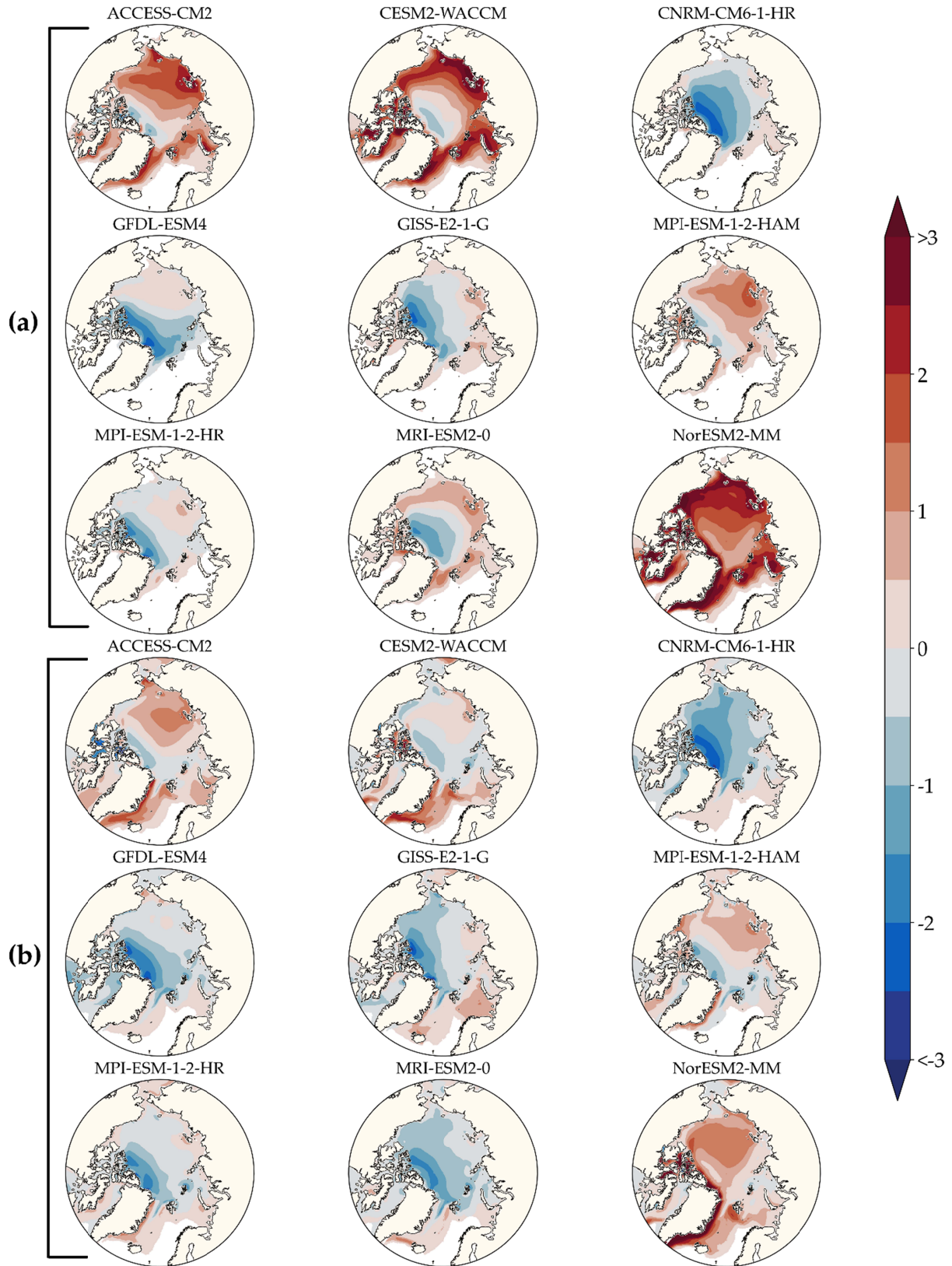
253

254 **Table 3. Statistics of error between each model's ensemble average and the reference**
 255 **PIOMAS reanalysis SIT for the individual months of September and March; and an**
 256 **average of all months 1979 through 2014. RMSE and Mean Bias have a unit of meters.**

MODEL	ACCESS- CM2	CESM2- WACCM	CNRM- CM6-1-HR	GFDL- ESM4	GISS- E2-1-G	MPI-ESM- 1-2-HAM	MPI-ESM- 1-2-HR	MRI- ESM2-0	NorESM 2-MM
SEPTEMBER									
<i>RMSE</i>	1.04	1.57	1.02	0.90	0.68	0.66	0.64	0.70	2.01
<i>MEAN BIAS</i>	0.68	1.05	-0.68	-0.59	-0.30	0.31	-0.30	0.07	1.65
<i>R</i>	0.72	0.45	0.82	0.75	0.87	0.84	0.87	0.76	0.67
MARCH									
<i>RMSE</i>	0.76	0.89	0.93	0.84	0.67	0.60	0.67	0.69	1.31
<i>MEAN BIAS</i>	0.27	0.15	-0.60	-0.53	-0.23	0.01	-0.24	-0.42	0.77
<i>R</i>	0.83	0.73	0.87	0.86	0.89	0.87	0.88	0.93	0.78
ANNUAL									
<i>RMSE</i>	0.91	1.13	0.96	0.83	0.66	0.60	0.65	0.73	1.61
<i>MEAN BIAS</i>	0.46	0.44	-0.63	-0.51	-0.23	0.12	-0.24	-0.21	1.11
<i>R</i>	0.78	0.62	0.85	0.84	0.89	0.87	0.87	0.82	0.73

257

258



260 **Figure 2. Sea ice thickness bias (meters) between model ensemble mean and PIOMAS for**
 261 **October (a) and March (b), over the period 2011-2014.**

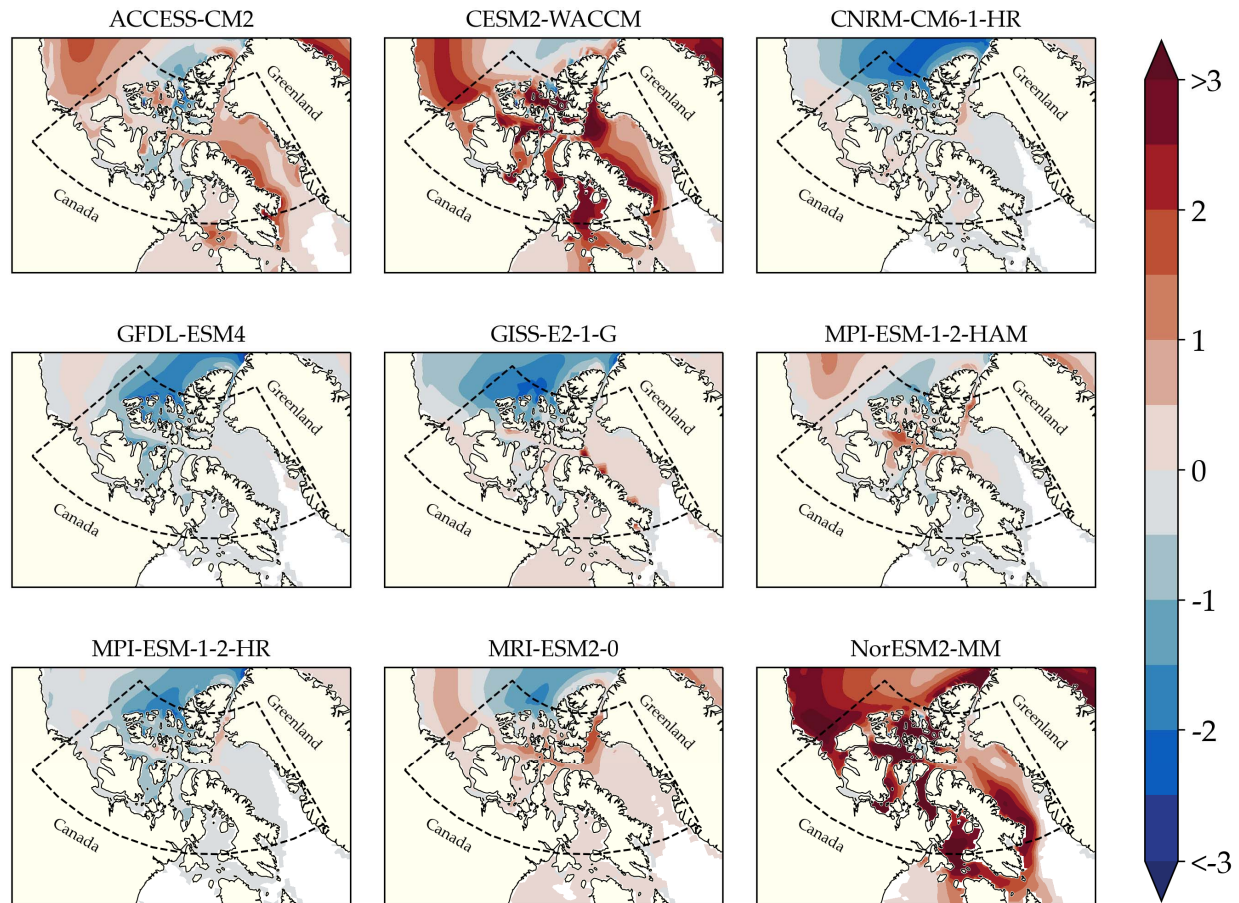
262 3.2 Canadian Archipelago Sea Ice Thickness

263 CMIP6 climate models have demonstrated positive biases for SIT within the Canadian
 264 Archipelago (Davy & Outten, 2020). Investigating the performance of individual models in this
 265 region is relevant to understanding future development and maritime travel along Arctic sea
 266 routes such as the Northwest Passage. Analysis we performed in comparison to PIOMAS and the
 267 localized summary statistics in this area defined by latitudes 60°N to 80°N and longitudes 50°W
 268 to 130°W can be seen in Table 3. CNRM-CM6-1-HR, GFDL-ESM4, GISS-E2-1-G, and MPI-
 269 ESM-1-2-HAM models have correlation coefficient $r \geq 0.8$, with MPI-ESM-1-2-HAM having
 270 the lowest RMSE (as it did for the pan-Arctic assessment). The majority of models show positive
 271 bias through most of the Canadian Archipelago, yet the three models with highest resolution
 272 (CNRM-CM6-1-HR, GFDL-ESM4, MPI-ESM-1-2-HR) trend toward negative bias for most of
 273 the region. These three models have similar SIT spatial distributions as seen in Figure 3 and
 274 possess strong negative bias in the Queen Elizabeth Islands in the northern part of the
 275 archipelago. GISS-E2-1-G trends toward overestimation of SIT throughout the region with
 276 several isolated locations of intense SIT along the western part of Baffin Bay. As the model with
 277 coarsest spatial resolution, GISS-E2-1-G's high correlation coefficient, comparable to that of the
 278 high-resolution models (CNRM-CM6-1-HR, MPI-ESM-1-2-HR) is unexpected – as model
 279 resolution would be expected to be a key factor in simulating sea ice dynamics within the region
 280 (Docquier et al., 2019). Within the northern part of the Canadian Archipelago, CESM2-WACCM
 281 simulates localized extreme SIT values exceeding 10 meters; this in part drives the poor spatial
 282 correlation and high error statistics for this model. By applying a SIT cutoff at 6m (such as that
 283 applied by Watts et al. (Watts et al., 2021)) the model performance is improved markedly, as the
 284 correlation coefficient rises to 0.52 while RMSE and mean bias fall to 1.3m and 44cm
 285 respectively.

286 **Table 4. Regional Summary statistics of error for the Canadian Archipelago and Baffin**
 287 **Bay between each climate model and the reference PIOMAS SIT compared September**
 288 **1979 - 2014. Mean, and RMSE have a unit of meters.**

MODEL	ACCESS- CM2	CESM2- WACCM	CNRM- CM6-1-HR	GFDL- ESM4	GISS- E2-1-G	MPI-ESM- 1-2-HAM	MPI-ESM- 1-2-HR	MRI- ESM2-0	NorESM 2-MM
SEPTEMBER									
<i>RMSE</i>	0.93	1.70	0.90	0.98	0.72	0.62	0.74	0.69	1.81
<i>MEAN BIAS</i>	-0.01	0.53	-0.62	-0.75	-0.29	-0.07	-0.34	-0.09	0.95
<i>R</i>	0.61	0.45	0.80	0.80	0.80	0.82	0.78	0.77	0.64

289



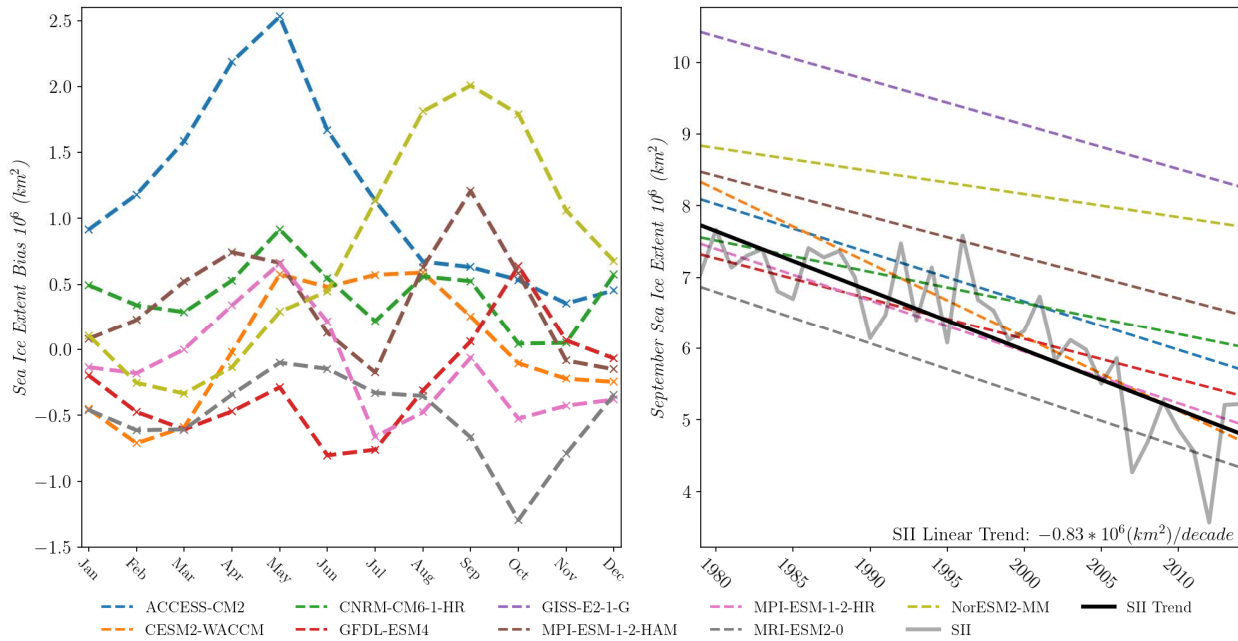
290

291 **Figure 3. Sea ice thickness bias (meters) between model ensemble mean and PIOMAS for**
 292 **September within the Canadian Archipelago 1979 -2014. The delineation boundary is**
 293 **shown for selection of data used in deriving statistical measures.**

294 3.3 Sea Ice Extent

295 Sea ice coverage within the Arctic is a critical parameter in governing Arctic surface
 296 exchange of heat, mass, and momentum and thus has been the topic of several CMIP6 and
 297 CMIP5 studies (Shen et al., 2021; Shu et al., 2020). The current generation of CMIP6 climate
 298 models typically over-represent SIE during both the seasonal maximum during March and the
 299 annual minimum during September (Shu et al., 2020). In this analysis, the majority of models
 300 overpredict SIE in summer months, yet are more evenly distributed during winter months as seen
 301 in Figure 4. One model, GISS-E2-1-G, shows considerably large positive bias throughout the
 302 year and peaking in March. CESM2-WACCM, GFDL-ESM4, CNRM-CM6-1-HR and MPI-
 303 ESM-1-2-HR have a mean absolute percentage error less than 4% annually and for September.
 304 These same models have the lowest September percent error among all models. GFDL-ESM4
 305 and MPI-ESM-1-2-HR are closest to the mean September SIE area, with 1% and -1% percent
 306 error respectively. The observed and simulated linear trends in SIE loss for the month of
 307 September 1979 - 2014 is shown in Figure 4b and corresponding statistics are provided in Table
 308 4. The best fit line to observed SII September SIE has a slope of $-0.83 \times 106 \text{ km}^2/\text{decade}$. The
 309 models with the nearest trend are MPI-ESM-1-2-HR and MRI-ESM2-0 – both having a rate of -

310 $0.72 \times 10^6 \text{ km}^2/\text{decade}$. All models except for CESM2-WACCM underpredict the rate of sea ice
 311 decline for this period – a trait previously observed common to most climate models (SIMIP
 312 Community, 2020).
 313



314
 315 **Figure 4. Average monthly SIE bias for each climate model over the period 1979 – 2014.**
 316 **(b): Observed and simulated SIE linear trend compared to the NSIDC record.**
 317 **GISS-E2-1-G is not shown in the plot (a), as error for this model exceeds $+2.5 \times 10^6 \text{ km}^2$**
 318 **for all months.**

320 **Table 5. Monthly percent error in comparison to the NSIDC observations and September**
 321 **SIE linear trend ($10^6 \text{ km}^2/\text{decade}$) through the period 1979 – 2014.**

MODEL:	ACCESS-CM2	CESM2-WACCM	CNRM-CM6-1-HR	GFDL-ESM4	GISS-E2-1-G	MPI-ESM-1-2-HAM	MPI-ESM-1-2-HR	MRI-ESM2-0	NorESM2-MM
March Percent Error	10%	-4%	2%	-4%	35%	3%	0.0%	-4%	-2%
September Percent Error	10%	4%	8%	1%	49%	19%	-1%	-11%	32%
Annual Percent Error	10%	1%	4%	-2%	40%	4%	-2%	-5%	9%
Mean Absolute % Error	9.8%	3.7%	3.9%	3.6%	39.7%	4.6%	3.3%	5.1%	9.9%
September SIE Linear Trend ($10^6 \text{ km}^2/\text{decade}$)	-0.68	-1.03	-0.44	-0.57	-0.62	-0.57	-0.72	-0.72	-0.32

322 **3.4 Surface Air Temperature**

323 The summary statistics derived from SAT analysis are presented in Table 5. Here,
 324 correlation coefficients are omitted from the statistical measure, as all models maintain annual
 325 correlation ≥ 0.97 when compared with ERA5 data. Examining mean error, all models except for
 326 MRI-ESM2-0 have negative annual bias. As previously mentioned, this is most likely driven by
 327 a previously acknowledged positive bias in ERA5 Arctic temperatures during the coldest winter

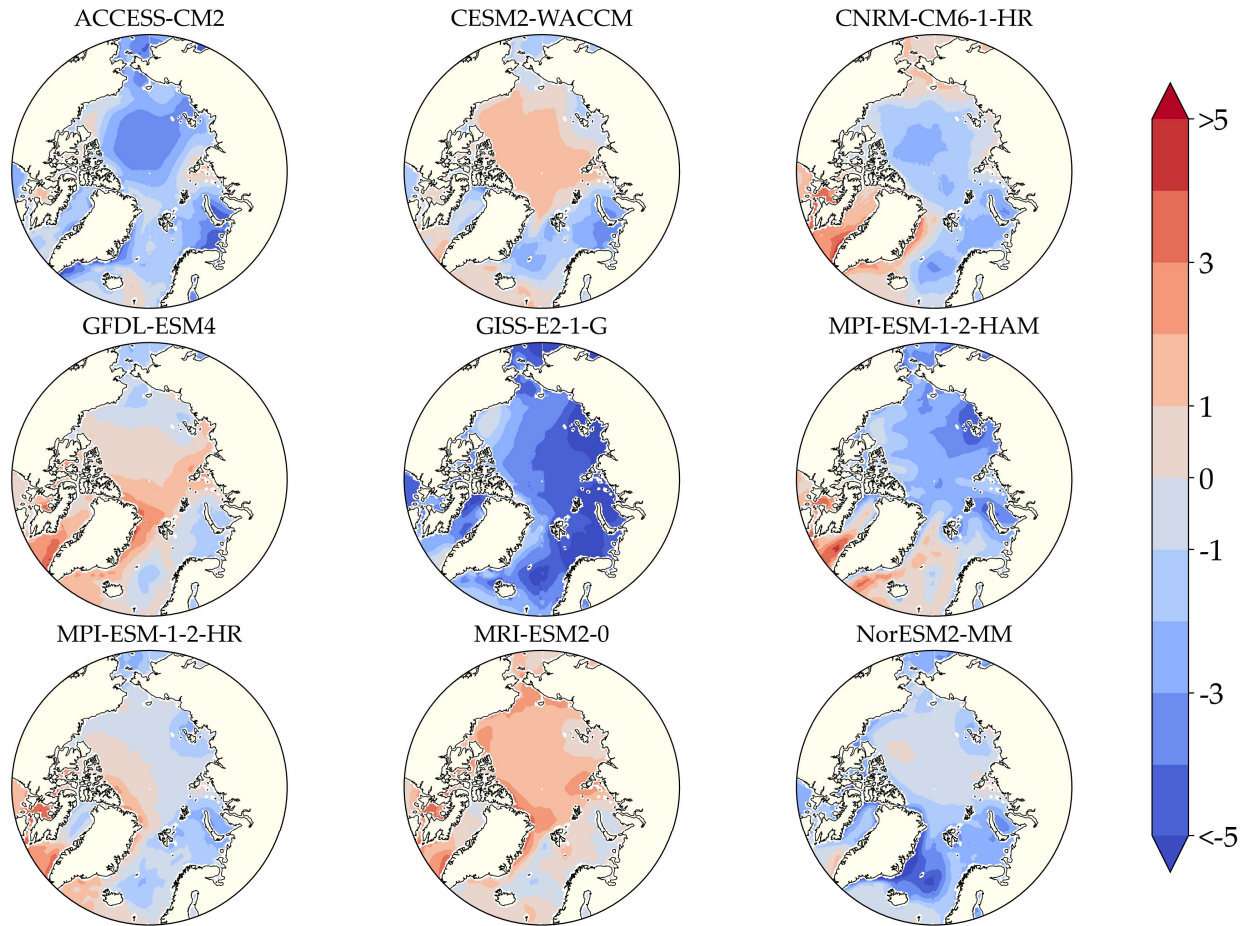
328 months and further evidenced by the large negative mean bias values for the month of the March
 329 shown in Table 5. Considering the potential effect this bias may have during colder months,
 330 assessment should prioritize September SAT performance where the ERA5 negative bias is not
 331 present and climate model mean bias values are more evenly distributed.

332

333 **Table 6. Summary statistics for each climate model's surface air temperature in Celsius**
 334 **(°C) compared with ERA5 monthly surface air temperature within the region from 1979 -**
 335 **2014.**

Model	ACCESS- CM2	CESM2- WACCM	CNRM- CM6-1-HR	GFDL- ESM4	GISS- E2-1-G	MPI-ESM- 1-2-HAM	MPI-ESM- 1-2-HR	MRI- ESM2-0	NorESM 2-MM
SEPTEMBER									
<i>RMSE</i>	2.5	1.5	1.7	1.2	4.1	2.4	1.0	1.6	1.6
<i>MEAN BIAS</i>	-2.2	0.6	-1.2	0.7	-3.9	-2.0	-0.1	1.4	-1.2
MARCH									
<i>RMSE</i>	7.2	3.0	6.6	6.1	8.7	5.8	2.4	1.6	5.8
<i>MEAN BIAS</i>	-6.8	-2.0	-5.9	-5.2	-7.8	-5.0	-1.7	-0.4	-5.3
ANNUAL									
<i>RMSE</i>	5.1	2.2	4.7	3.9	5.8	3.8	1.9	1.9	4.4
<i>MEAN BIAS</i>	-4.1	-0.8	-3.7	-2.4	-4.8	-2.9	-0.6	0.2	-3.5

336 Temperature bias contour maps for the month of September can be seen in Figure 5. For
 337 September, the model with the lowest RMSE and mean bias is MPI-ESM-1-2-HR at 1.0°C and
 338 -0.1°C respectively. Examining the spatial bias of this model in Figure 5, it overestimates
 339 temperature for most of the seas surrounding Greenland and within the Canadian Archipelago (a
 340 feature observed in the majority of models) yet has minimal underestimation for the remainder of
 341 the Arctic. CNRM-CM6-1-HR, GFDL-ESM4, MPI-ESM-1-2-HAM, MPI-ESM-1-2-HR, and
 342 MRI-ESM2-0 all exhibit similar trends in high positive bias through the Canadian Archipelago,
 343 Baffin Bay, and the Greenland Sea. GISS-E2-1G, ACCESS-CM2 and MPI-ESM-1-2-HAM have
 344 consistent Pan-Arctic negative bias while ACCESS-CM2 and MPI-ESM-1-2-HAM also have
 345 large areas of negative bias reaching from the North Pole through the East Siberian and into the
 346 Bearing Sea. MRI-ESM2-0 has the lowest mean annual bias of 0.2°C and is even with MPI-
 347 ESM-1-2-HR with the lowest annual RMSE of 1.9°C. Investigating this result, the model shows
 348 minimal error during winter months (a result potentially driven by positive bias in ERA5 winter
 349 temperatures and discussed in section 4) as shown for the month of March in Table 5. The
 350 previously discussed SAT positive bias within ERA5 under extreme cold weather may have had
 351 significant influence in this result and thus demand future investigation and confirmation.



352

353 **Figure 5. Surface air temperature bias for the month of September averaged over 1979-**
 354 **2014. Temperatures over land have been excluded from analysis and masked over for**
 355 **mapping.**

356 3.5 Surface Wind Speed

357 Analysis of SWS yields the summary statistics shown in Table 6. The spread in annual
 358 RMSE between models is less than 0.7 m/s and the range in annual bias values does not exceed 2
 359 m/s. MPI-ESM-1-2-HR maintains the lowest RMSE out of all the models for September, March,
 360 and annually. Most models (excepting NorESM2-MM) show improved correlation for March in
 361 comparison to September, with GFDL-ESM4 experiencing the largest improvement.

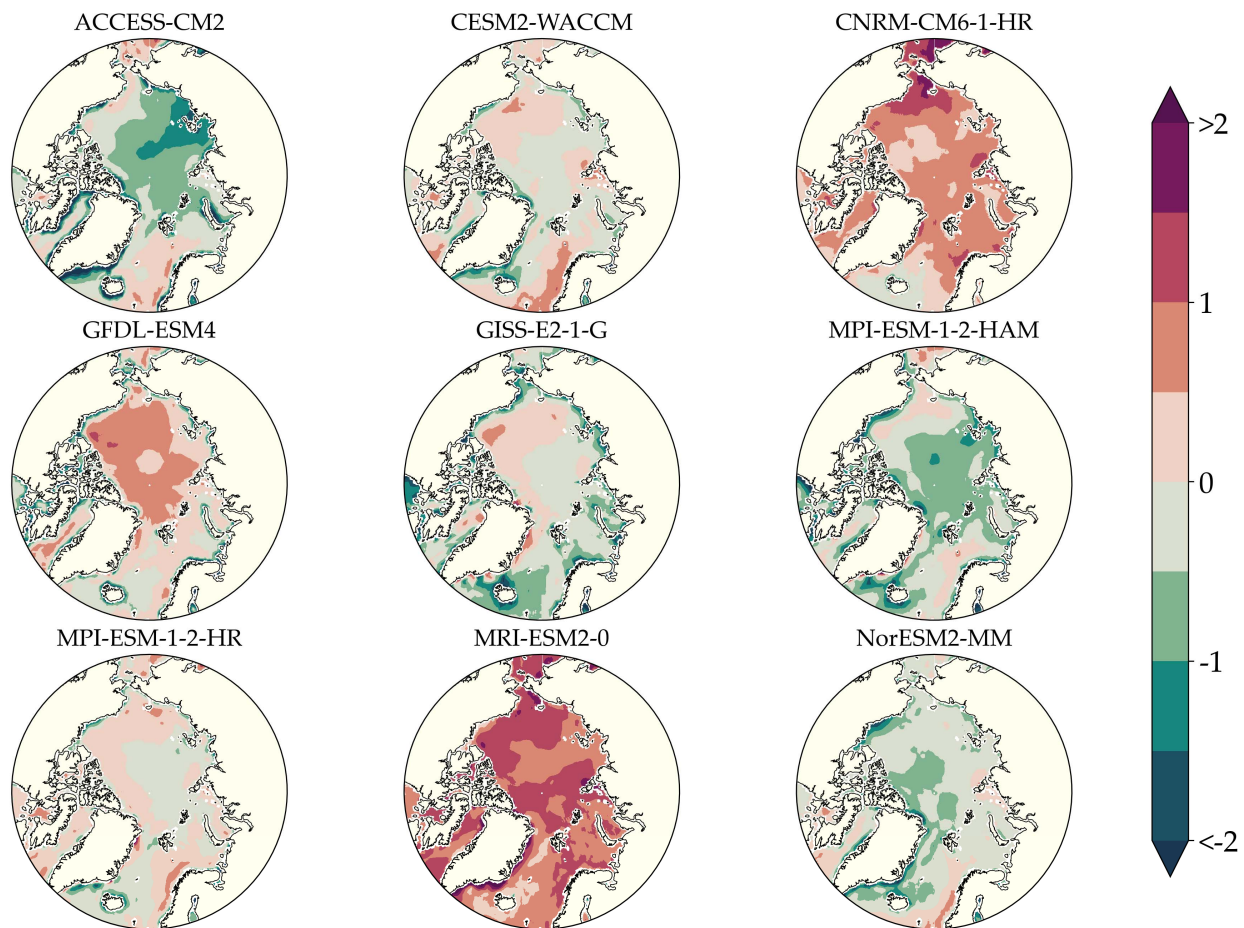
362 In Figure 6, the spatial bias contours can be used to elucidate the September statistics
 363 provided in Table 6. CNRM-CM6-1-HR and MRI-ESM2-0 immediately stand out as exhibiting
 364 pervasive positive bias for not only oceanic regions but also within coastal areas. A common
 365 feature in many of the models shown is a tendency for coastal areas to have considerable
 366 negative bias. This can be observed for the majority of models in the Beaufort Sea or along the
 367 southeast coast of Greenland. MPI-ESM-1-2-HR shows noticeably little bias exceeding 0.5m/s,
 368 demonstrating the accuracy of the model.

369

370 **Table 7. Summary statistics for each climate model's surface wind speed simulation with**
 371 **ERA-5 monthly surface wind speed within the region north of 60°N from 1979 to 2014.**
 372 **RMSE and mean bias have units of m/s.**

MODEL	ACCESS- CM2	CESM2- WACCM	CNRM- CM6-1-HR	GFDL- ESM4	GISS- E2-1-G	MPI-ESM- 1-2-HAM	MPI-ESM- 1-2-HR	MRI- ESM2-0	NorESM 2-MM
SEPTEMBER									
<i>RMSE</i>	0.79	0.33	0.68	0.63	0.49	0.70	0.29	1.02	0.51
<i>MEAN BIAS</i>	-0.63	-0.08	0.62	0.35	-0.24	-0.60	-0.05	0.99	-0.41
<i>R</i>	0.90	0.93	0.93	0.75	0.84	0.91	0.93	0.95	0.95
MARCH									
<i>RMSE</i>	0.69	0.68	0.46	0.51	0.74	0.57	0.44	1.27	1.03
<i>MEAN BIAS</i>	-0.40	-0.42	0.21	0.13	-0.37	-0.40	-0.19	1.22	-0.92
<i>R</i>	0.91	0.94	0.96	0.93	0.88	0.96	0.96	0.97	0.95
ANNUAL									
<i>RMSE</i>	0.75	0.63	0.56	0.54	0.62	0.69	0.41	1.07	0.94
<i>MEAN BIAS</i>	-0.51	-0.39	0.37	0.13	-0.23	-0.54	-0.16	0.99	-0.73
<i>R</i>	0.90	0.93	0.94	0.90	0.88	0.95	0.95	0.96	0.89

373



374

375 **Figure 6. Monthly surface wind speed bias averaged for all months 1979 through 2014.**
 376 **Only surface winds corresponding to oceanic grid cells were considered for analysis.**

377 **4 Discussion and Conclusion**

378 Assessment of climate model historical simulation of SIT shows that the spatial
 379 distribution diverges greatly between models. Mean annual SIT bias derived from comparison to

380 PIOMAS ranges from -0.63m to 1.11m and the comparison from CS2SMOS yields winter SIT
381 bias ranging from -0.2m to 0.81m. Models have improved spatial correlation with PIOMAS over
382 CS2SMOS; these results are partially expected, as PIOMAS shares several regions of inaccurate
383 simulated SIT common to the climate models (J. Stroeve et al., 2014). Yet this may also stem
384 from the brevity of the CS2SMOS time series used to establish the mean monthly SIT
385 distribution and the inclusion of the anomalous 2012 September sea ice minimum. Despite the
386 considerable inter-model variance observed, there are several trends common to the majority of
387 models. Foremost, many of the models that otherwise show minimal error throughout most of the
388 Arctic, fail to simulate the thickest sea ice regimes at the Lincoln Sea and extending towards
389 north of the Canadian Archipelago. This strong negative bias ($\leq -1\text{m}$) is present year-round for
390 more than half the models. Notably, however, this bias is reduced for CS2SMOS in comparison
391 to PIOMAS; suggesting that the models are perhaps more capable of simulating thinner ice
392 (more sensitive to climate and oceanic forcing (Overland, 2020)) in the latter part of the time
393 series.

394 Examining SIE simulation skill, all models are capable of simulating the basic features of
395 the seasonal cycle, with maximum extent occurring in March and the minimum occurring in
396 September. Most models exhibit positive bias for September and reduced error for March.
397 Examining trends in September SIE, all models except for one (CESM2-WACCM)
398 underestimate the rate of sea ice decline by at least $0.1 \text{ km}^2/\text{decade}$. Both these results are in
399 agreement with other studies showing that CMIP6 climate models generally underestimate the
400 rate of sea ice retreat and struggle to capture the annual sea ice minimum. The MPI-ESM-1-2-
401 HR ensemble average has very little bias for September mean SIE, the lowest annual absolute
402 mean percentage error, and a comparable September SIE trend through the time series.

403 SAT comparison between climate models and ERA5 shows that nearly all models have
404 an annual cold bias. This result is believed to have been driven by a warm bias present in the
405 ERA5 dataset used in climate model assessment. Several studies have confirmed that ERA5 or
406 ERA-Interim (predecessor to ERA5) possesses a sizeable Arctic SAT warm bias ($+3.9^\circ\text{C}$ to
407 $+5.4^\circ\text{C}$) during the winter months in extreme cold weather conditions (Demchev et al., 2020;
408 Graham et al., 2019; C. Wang et al., 2019). The exact spatial and temporal characteristics of this
409 warm bias are unclear and thus cannot be corrected; yet it is clear that the warm bias grows as air
410 temperatures become colder, peaking in winter months at high latitudes. For this reason,
411 emphasis in assessment should be placed on warmer months, such as the metrics derived for
412 September. For September, the range of bias spans from -3.9°C to 1.4°C for the models GISS-
413 E2-1-G and MRI-ESM2-0 respectively. For March, the inter-model bias ranges from -0.4°C to -
414 7.8°C – yet the significance of these results are questionable given the acknowledged ERA5 bias.
415 It is recommended that an alternative data source be used for SAT analysis in future analysis.
416 Multiple atmospheric reanalysis products have been shown to possess a similar warm bias during
417 extreme cold temperatures (Graham et al., 2019); however, this trend is especially pertinent in
418 ERA5. Otherwise, the use of in situ data could be considered for comparison at the cost of losing
419 spatial coverage and continuous data availability. Model simulations of wind show that most
420 models have reliably high correlation values and annual bias not exceeding 1m/s . Most models
421 commonly underestimate SWS in coastal areas and only two models exhibit a pervasive positive
422 bias. MPI-ESM-1-2-HR has the lowest RMSE through all seasons and the highest annual
423 correlation.

424 Climate model simulation of historical Arctic sea ice thickness, extent, surface wind
425 speed, and temperature were analyzed against satellite, sea ice reanalysis, and atmospheric
426 reanalysis data to derive skill metric statistic and bias contour maps. Coupled climate models
427 represent an invaluable source of future climate data for regional modeling and research efforts.
428 Individual climate models participating within CMIP6 may diverge substantially in ability to
429 simulate historical sea ice and related climate variables, thus contributing to the uncertainty in
430 projecting the future sea ice decline. By this rational, the evaluation and understanding of
431 individual model historical simulation is desirable. Models were shown to present considerable
432 differences in simulating the spatial distribution of SIT within the Arctic and no one model could
433 be identified as presenting a totally resolved sea ice distribution representing observed
434 conditions. Nonetheless, results and conclusions of this study contribute to the body of
435 knowledge of climate model performance and may be used to inform model selection for reliant
436 Arctic research. In comparison to CS2SMOS satellite data, MPI-ESM-1-2-HR led in all
437 performance metrics overall and presented competitive performance in comparison to PIOMAS.
438 For SAT, MRI-ESM2-0 presents the lowest annual mean bias and RMSE; however, this result is
439 contentious due to a strong warm bias within the ERA5 data for winter months. Considering the
440 rapid climate change in the Arctic, the ability to accurately predict the evolution and decline of
441 sea ice within this region is crucial to predicting the timeline and scope of effects that will be felt
442 worldwide. The findings in this study are presented with the intention of aiding regional Arctic
443 research reliant on climate model forecasting data.

444 **Acknowledgments**

445 This material is based upon work supported by the National Science Foundation under
446 Grant No. # 1927785. This funding is gratefully acknowledged but implies no endorsement of
447 the findings. The authors would also like to thank NSF for the scholarships to the first, fourth,
448 and fifth authors
449

450 **Open Research**

451 The climate model data from the World Climate Research Programme used within this
452 study is freely available at: <https://esgf-node.llnl.gov/projects/cmip6/> . Merged CryoSat-
453 2/SMOS sea ice thickness is accessible via <https://spaces.awi.de/display/CS2SMOS> and
454 PIOMAS sea ice thickness can be accessed through <http://psc.apl.uw.edu/data/> . ERA5 surface
455 wind speed and air temperature are available at <https://cds.climate.copernicus.eu/> .
456

457 **References**

458 Aksenov, Y., Popova, E. E., Yool, A., Nurser, A. J. G., Williams, T. D., Bertino, L., & Bergh, J.
459 (2017). On the future navigability of Arctic sea routes: High-resolution projections of the Arctic
460 Ocean and sea ice. *Marine Policy*, 75, 300–317. <https://doi.org/10.1016/j.marpol.2015.12.027>

461

462 Barnhart, K. R., Overeem, I., & Anderson, R. S. (2014). The effect of changing sea ice on the
463 physical vulnerability of Arctic coasts. *Cryosphere*, 8(5), 1777–1799. [https://doi.org/10.5194/tc-](https://doi.org/10.5194/tc-8-1777-2014)
464 8-1777-2014

465

466 Casas-Prat, M., Wang, X. L., & Swart, N. (2018). CMIP5-based global wave climate projections
467 including the entire Arctic Ocean. *Ocean Modelling*, 123(January), 66–85.
468 <https://doi.org/10.1016/j.ocemod.2017.12.003>

469

470 Casas-Prat, Mercè, & Wang, X. L. (2020). Sea Ice Retreat Contributes to Projected Increases in
471 Extreme Arctic Ocean Surface Waves. *Geophysical Research Letters*, 47(15).
472 <https://doi.org/10.1029/2020GL088100>

473

474 Chen, J., Kang, S., Chen, C., You, Q., Du, W., Xu, M., Zhong, X., Zhang, W., & Jizu, C. (2020).
475 Changes in sea ice and future accessibility along the Arctic Northeast Passage. *Global and*
476 *Planetary Change*, 195, 103319. <https://doi.org/10.1016/j.gloplacha.2020.103319>

477

478 Davy, R., & Outten, S. (2020). The arctic surface climate in CMIP6: Status and developments
479 since CMIP5. *Journal of Climate*, 33(18), 8047–8068. <https://doi.org/10.1175/JCLI-D-19-0990.1>

480

481 Demchev, D. M., Kulakov, M. Y., Makshtas, A. P., Makhotina, I. A., Fil'chuk, K. V., & Frolov,
482 I. E. (2020). Verification of ERA-Interim and ERA5 Reanalyses Data on Surface Air
483 Temperature in the Arctic. *Russian Meteorology and Hydrology*, 45(11), 771–777.

484

485 Docquier, D., Grist, J. P., Roberts, M. J., Roberts, C. D., Semmler, T., Ponsoni, L., Massonnet,
486 F., Sidorenko, D., Sein, D. V., Iovino, D., Bellucci, A., & Fichefet, T. (2019). Impact of model
487 resolution on Arctic sea ice and North Atlantic Ocean heat transport. *Climate Dynamics*, 53(7–
488 8), 4989–5017. <https://doi.org/10.1007/s00382-019-04840-y>

489

490 Docquier, D., & Koenigk, T. (2021). Observation-based selection of climate models projects
491 Arctic ice-free summers around 2035. *Communications Earth and Environment*, 2(1), 1–8.
492 <https://doi.org/10.1038/s43247-021-00214-7>

493

494 Doscher, R., Vihma, T., & Maksimovich, E. (2014). Recent advances in understanding the Arctic
495 climate system state and change from a sea ice perspective: a review. *Atmospheric Chemistry
496 and Physics*, 14(24), 13571–13600.

497

498 Goosse, H., Kay, J. E., Armour, K. C., Bodas-Salcedo, A., Chepfer, H., Docquier, D., Jonko, A.,
499 Kushner, P. J., Lecomte, O., Massonnet, F., Park, H. S., Pithan, F., Svensson, G., &
500 Vancoppenolle, M. (2018). Quantifying climate feedbacks in polar regions. *Nature
501 Communications*, 9(1). <https://doi.org/10.1038/s41467-018-04173-0>

502

503 Graham, R. M., Cohen, L., Ritzhaupt, N., Segger, B., Graverson, R. G., Rinke, A., Walden, V.
504 P., Granskog, M. A., & Hudson, S. R. (2019). Evaluation of Six Atmospheric Reanalyses over
505 Arctic Sea Ice from Winter to Early Summer. *Journal of Climate*, 32(14), 4121–4143.

506

- 507 Haine, T. W. N., Curry, B., Gerdes, R., Hansen, E., Karcher, M., Lee, C., Rudels, B., Spreen, G.,
508 de Steur, L., Stewart, K. D., & Woodgate, R. (2015). Arctic freshwater export: Status,
509 mechanisms, and prospects. *Global and Planetary Change*, 125, 13–35.
510 <https://doi.org/10.1016/j.gloplacha.2014.11.013>
511
- 512 Harsem, Ø., Heen, K., Rodrigues, J. M. P., & Vassdal, T. (2015). Oil exploration and sea ice
513 projections in the Arctic. *Polar Record*, 51(1), 91–106.
514
- 515 Karlsson, J., & Svensson, G. (2013). Consequences of poor representation of Arctic sea-ice
516 albedo and cloud-radiation interactions in the CMIP5 model ensemble. *Geophysical Research*
517 *Letters*, 40(16). <https://doi.org/10.1002/grl.50768>
518
- 519 Knutti, R., Sedláček, J., Sanderson, B. M., Lorenz, R., Fischer, E. M., & Eyring, V. (2017). A
520 climate model projection weighting scheme accounting for performance and interdependence.
521 *Geophysical Research Letters*, 44(4), 1909–1918. <https://doi.org/10.1002/2016GL072012>
522
- 523 Kwok, R. (2018). Arctic sea ice thickness, volume, and multiyear ice coverage: Losses and
524 coupled variability (1958-2018). In *Environmental Research Letters* (Vol. 13, Issue 10). Institute
525 of Physics Publishing. <https://doi.org/10.1088/1748-9326/aae3ec>
526
- 527 Kwok, R., & Cunningham, G. F. (2015). Variability of arctic sea ice thickness and volume from
528 CryoSat-2. *Philosophical Transactions of the Royal Society A: Mathematical, Physical and*
529 *Engineering Sciences*, 373(2045). <https://doi.org/10.1098/rsta.2014.0157>

530

531 Kwok, R., Spreen, G., & Pang, S. (2013). Arctic sea ice circulation and drift speed: Decadal
532 trends and ocean currents: ARCTIC SEA ICE MOTION. *Journal of Geophysical Research.*
533 *Oceans*, 118(5), 2408–2425.

534

535 Laxon, S. W., Giles, K. A., Ridout, A. L., Wingham, D. J., Willatt, R., Cullen, R., Kwok, R.,
536 Schweiger, A., Zhang, J., Haas, C., Hendricks, S., Krishfield, R., Kurtz, N., Farrell, S., &
537 Davidson, M. (2013). CryoSat-2 estimates of Arctic sea ice thickness and volume. *Geophysical*
538 *Research Letters*, 40(4), 732–737. <https://doi.org/10.1002/grl.50193>

539

540 Lindsay, R., Wensnahan, M., Schweiger, A., & Zhang, J. (2014). Evaluation of seven different
541 atmospheric reanalysis products in the arctic. *Journal of Climate*, 27(7), 2588–2606.
542 <https://doi.org/10.1175/JCLI-D-13-00014.1>

543

544 Long, M., Zhang, L., Hu, S., & Qian, S. (2021). Multi-aspect assessment of cmip6 models for
545 arctic sea ice simulation. *Journal of Climate*, 34(4), 1515–1529. [https://doi.org/10.1175/JCLI-D-](https://doi.org/10.1175/JCLI-D-20-0522.1)
546 [20-0522.1](https://doi.org/10.1175/JCLI-D-20-0522.1)

547

548 Maslanik, J. A., Fowler, C., Stroeve, J., Drobot, S., Zwally, J., Yi, D., & Emery, W. (2007). A
549 younger, thinner Arctic ice cover: Increased potential for rapid, extensive sea-ice loss.
550 *Geophysical Research Letters*, 34(24), L24501-n/a.

551

552 Meier, W., Fetterer, F., Savoie, M., Mallory, S., Duerr, R., & Stroeve, J. (2017). NOAA/NSIDC
553 Climate Data Record of Passive Microwave Sea Ice Concentration. In Boulder, Colorado USA:
554 National Snow and Ice Data Center. [https://doi.org/https://doi.org/10.7265/N59P2ZTG](https://doi.org/10.7265/N59P2ZTG)
555

556 Melia, N., Haines, K., & Hawkins, E. (2016). Sea ice decline and 21st century trans-Arctic
557 shipping routes. *Geophysical Research Letters*, 43(18), 9720–9728.
558

559 Mioduszewski, J., Vavrus, S., & Wang, M. (2018). Diminishing Arctic sea ice promotes stronger
560 surface winds. *Journal of Climate*, 31(19), 8101–8119. <https://doi.org/10.1175/JCLI-D-18->
561 0109.1
562

563 Olason, E., & Notz, D. (2014). Drivers of variability in Arctic sea-ice drift speed. *Journal of*
564 *Geophysical Research. Oceans*, 119(9), 5755–5775.
565

566 Overland, J. E. (2020). Less climatic resilience in the Arctic. *Weather and Climate Extremes*, 30,
567 100275-
568

569 Peng, G., Meier, W. N., Scott, D. J., & Savoie, M. H. (2013). A long-term and reproducible
570 passive microwave sea ice concentration data record for climate studies and monitoring. *Earth*
571 *System Science Data*, 5(2), 311–318. <https://doi.org/10.5194/essd-5-311-2013>
572

- 573 Ricker, R., Hendricks, S., Kaleschke, L., Tian-Kunze, X., King, J., & Haas, C. (2017). A weekly
574 Arctic sea-ice thickness data record from merged CryoSat-2 and SMOS satellite data. *The*
575 *Cryosphere*, 11(4), 1607–1623. <https://doi.org/10.5194/tc-11-1607-2017>
576
- 577 Schweiger, A. J., Steele, M., Zhang, J., Moore, G. W. K., & Laidre, K. L. (2021). Accelerated
578 sea ice loss in the Wandel Sea points to a change in the Arctic's Last Ice Area. *Communications*
579 *Earth & Environment*, 2(1), 1–12. <https://doi.org/10.1038/s43247-021-00197-5>
580
- 581 Schweiger, A., Lindsay, R., Zhang, J., Steele, M., Stern, H., & Kwok, R. (2011). Uncertainty in
582 modeled Arctic sea ice volume. *Journal of Geophysical Research: Oceans*, 116(9), 1–21.
583 <https://doi.org/10.1029/2011JC007084>
584
- 585 Shen, Z., Duan, A., Li, D., & Li, J. (2021). Assessment and ranking of climate models in Arctic
586 Sea ice cover simulation: From CMIP5 to CMIP6. *Journal of Climate*, 34(9), 3609–3627.
587 <https://doi.org/10.1175/JCLI-D-20-0294.1>
588
- 589 Shu, Q., Wang, Q., Song, Z., Qiao, F., Zhao, J., Chu, M., & Li, X. (2020). Assessment of Sea Ice
590 Extent in CMIP6 With Comparison to Observations and CMIP5. *Geophysical Research Letters*,
591 47(9). <https://doi.org/10.1029/2020GL087965>
592
- 593 Sibul, G., & Jin, J. G. (2021). Evaluating the feasibility of combined use of the Northern Sea
594 Route and the Suez Canal Route considering ice parameters. *Transportation Research Part A:*
595 *Policy and Practice*, 147(March), 350–369. <https://doi.org/10.1016/j.tra.2021.03.024>

596

597 SIMIP Community. (2020). Arctic Sea Ice in CMIP6. *Geophysical Research Letters*, 47(10).

598 <https://doi.org/10.1029/2019GL086749>

599

600 Stroeve, J., Barrett, A., Serreze, M., & Schweiger, A. (2014). Using records from submarine,
601 aircraft and satellites to evaluate climate model simulations of Arctic sea ice thickness.

602 *Cryosphere*, 8(5), 1839–1854. <https://doi.org/10.5194/tc-8-1839-2014>

603

604 Stroeve, Julienne, & Notz, D. (2018). Changing state of Arctic sea ice across all seasons. In
605 *Environmental Research Letters* (Vol. 13, Issue 10). Institute of Physics Publishing.

606 <https://doi.org/10.1088/1748-9326/aade56>

607

608 Thomson, J., & Rogers, W. E. (2014). Swell and sea in the emerging Arctic Ocean. *Geophysical*
609 *Research Letters*, 41(9), 3136–3140. <https://doi.org/10.1002/2014GL059983>

610

611 Timmermans, M. L., & Marshall, J. (2020). Understanding Arctic Ocean Circulation: A Review
612 of Ocean Dynamics in a Changing Climate. *Journal of Geophysical Research: Oceans*, 125(4),

613 1–35. <https://doi.org/10.1029/2018JC014378>

614

615 Tschudi, M. A., Stroeve, J. C., & Stewart, J. S. (2016). Relating the Age of Arctic Sea Ice to its
616 Thickness, as Measured during NASA's ICESat and IceBridge Campaigns. *Remote Sensing*

617 (Basel, Switzerland), 8(6), 457.

618

619 Wang, C., Graham, R. M., Wang, K., Gerland, S., & Granskog, M. A. (2019). Comparison of
620 ERA5 and ERA-Interim near-surface air temperature, snowfall and precipitation over Arctic sea
621 ice: effects on sea ice thermodynamics and evolution. *The Cryosphere*, 13(6), 1661–1679.
622 <https://doi.org/10.5194/tc-13-1661-2019>

623

624 Wang, X., Key, J., Kwok, R., & Zhang, J. (2016). Comparison of Arctic sea ice thickness from
625 satellites, aircraft, and PIOMAS data. *Remote Sensing*, 8(9). <https://doi.org/10.3390/rs8090713>

626

627 Watts, M., Maslowski, W., Lee, Y. J., Kinney, J. C., & Osinski, R. (2021). A spatial evaluation
628 of arctic Sea ice and regional limitations in CMIP6 historical simulations. *Journal of Climate*,
629 34(15), 6399–6420. <https://doi.org/10.1175/JCLI-D-20-0491.1>

630

631 Wei, T., Yan, Q., Qi, W., Ding, M., & Wang, C. (2020). Projections of Arctic sea ice conditions
632 and shipping routes in the twenty-first century using CMIP6 forcing scenarios. *Environmental*
633 *Research Letters*, 15(10).

634

635 Williams, D. M., & Erikson, L. H. (2021). Knowledge Gaps Update to the 2019 IPCC Special
636 Report on the Ocean and Cryosphere: Prospects to Refine Coastal Flood Hazard Assessments
637 and Adaptation Strategies With At-Risk Communities of Alaska. *Frontiers in Climate*,
638 3(December), 1–11. <https://doi.org/10.3389/fclim.2021.761439>

639

640 Zhang, J., & Rothrock, D. A. (2003). Modeling global sea ice with a thickness and enthalpy
641 distribution model in generalized curvilinear coordinates. *Monthly Weather Review*, 131(5),
642 845–861. [https://doi.org/10.1175/1520-0493\(2003\)131<0845:MGSIWA>2.0.CO;2](https://doi.org/10.1175/1520-0493(2003)131<0845:MGSIWA>2.0.CO;2)